

Characterizing many-body localization via exact disorder-averaged quantum noise

Michael Sonner,^{1,*} Alessio Lerose,^{1,*} and Dmitry A. Abanin¹

¹*Department of Theoretical Physics, University of Geneva,
Quai Ernest-Ansermet 24, 1205 Geneva, Switzerland*

(Dated: 3rd January 2022)

Many-body localized (MBL) phases of disordered quantum many-particle systems have a number of unique properties, including failure to act as a thermal bath and protection of quantum coherence. Studying MBL is complicated by the effects of rare ergodic regions, necessitating large system sizes and averaging over many disorder configurations. Here, building on the Feynman-Vernon theory of quantum baths, we characterize the quantum noise that a disordered spin system exerts on its parts via an influence matrix (IM). In this approach, disorder averaging is implemented exactly, and the thermodynamic-limit IM obeys a self-consistency equation. Viewed as a wavefunction in the space of trajectories of an individual spin, the IM exhibits slow scaling of temporal entanglement in the MBL phase. This enables efficient matrix-product-states computations to obtain temporal correlations, providing a benchmark for quantum simulations of non-equilibrium matter. The IM quantum noise formulation provides an alternative starting point for novel rigorous studies of MBL.

Introduction — Many-body localization (MBL) in strongly disordered interacting quantum systems represents one of the rare known examples of a genuinely non-ergodic phase of quantum matter [1–3]. The phenomenology of the MBL phase [4–7], its persistence in periodically driven systems [8–10], and new phases of matter enabled by MBL [11] are being intensely investigated.

Unlike in conventional phase transitions, thermal ensembles bear no signatures of the MBL transition. Localization effects instead manifest themselves in the properties of individual highly-excited energy eigenstates, as well as in the coherent, far-from-equilibrium dynamics, which differ drastically from those in the thermalizing phase. In particular, MBL eigenstates exhibit boundary-law entanglement scaling [4, 12], similar to ground states of gapped systems [13]. Local memory of the initial state is preserved, owing to the emergence of local integrals of motion [4–7] – a signature that has been widely used to diagnose MBL in quantum quench experiments with ultracold atoms [14–16], trapped ions [17], and superconducting qubits [18].

The simultaneous presence of disorder and interactions, combined with a necessity to describe highly excited eigenstates, poses a major challenge for the theoretical description of MBL. Rigorous perturbative approaches are difficult, as they require treating disorder probabilistically [7] and incorporating the effects of rare regions [19]. Exact diagonalization (ED) studies [20–23] give access to excited eigenstates, but are limited in system size. Tensor-network approaches to MBL, relying on low real-space entanglement of MBL states, have been used to approximately construct eigenstates [24–27] and

simulate non-equilibrium dynamics [28] beyond the reach of ED. While such investigations gave insights into MBL physics, their power is limited by finite-size and/or -time effects, and by the practical cost of sampling disorder configurations.

In this Article, we introduce a method for describing *disorder-averaged* dynamical properties of many-body systems, and apply it to a periodically driven (Floquet) spin model of MBL. We characterize the system’s dynamics by its *influence matrix* (IM) [29], inspired by the Feynman-Vernon theory of a quantum particle interacting with a bath of harmonic oscillators [30, 31]. We use the IM to characterize how a quantum many-body system affects the time evolution of its local subsystems, i.e., how it acts as a “bath” on itself. An IM contains full information on temporal correlations of local operators, and can be viewed as a kind of generating functional of the system’s self-induced quantum noise. This formalism is advantageous for MBL, as it naturally accommodates the thermodynamic limit and *exact* disorder averaging.

In one-dimensional homogeneous systems, the IM can be found from a linear self-consistency equation [29, 32]. While individual realizations of disordered systems have IMs that depend on position, averaging over a translationally invariant disorder distribution leads to a translationally invariant IM. Disorder-averaging, however, leads to terms which are non-local in time in the self-consistency equation. Below we argue that, in spite of this nonlocality, the disorder-averaged IM of a MBL system is characterized by low *temporal entanglement*. This opens the door to efficient matrix-product states (MPS) methods for computing disorder-averaged dynam-

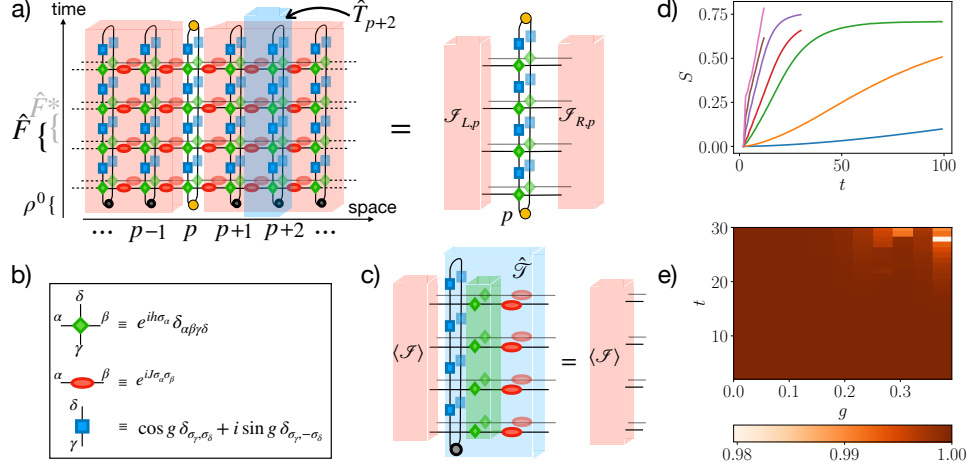


Figure 1. a) Circuit representation of a local temporal correlation function in the Keldysh path integral representation, Eq. (2), with circuit elements for model (1) defined in panel b). The two layers reflect forward and backward propagation of the system. Panel a) pictures Eq. (3). The blue shaded tensor represents the transfer matrix, defined in Eq. (4). Panel c) illustrates Eq. (5) (self-consistency equation). The green shaded tensor corresponds to non-local in time “interactions” arising from exact disorder averaging. d) Scaling of temporal entanglement of the IM for $J = g = 0.04, 0.08, 0.16, 0.20, 0.27$ (DMRG) and $J = g = 0.35, 0.51$ (ED), bottom to top. e) Expectation value of the transfer matrix applied to the MPS with bond dimension $\chi = 128$ obtained from DMRG.

ical properties. As a first application of the method, we compute the dynamical correlation functions of a MBL system up to long times.

The IM undergoes a drastic change when the system transitions from the ergodic to the MBL phase; MBL IMs are characterized by persistent quantum-interference effects, which express the fact that MBL systems are not efficient thermal baths. This can be viewed as the emergence of *temporal long-range order* in the statistical ensemble of local trajectories governed by the IM. Below, we will use an MPS approach to demonstrate this phenomenon [33].

Model — For concreteness, in this Article we will focus on the disordered kicked Ising chain (KIC), which provides a Floquet model of MBL [34, 35]. Time evolution of this system is governed by repeated applications of the Floquet operator,

$$\hat{F} = \exp\left(i \sum_j g \hat{\sigma}_j^x\right) \exp\left(i \sum_j J \hat{\sigma}_j^z \hat{\sigma}_{j+1}^z + h_j \hat{\sigma}_j^z\right), \quad (1)$$

where $\hat{\sigma}_j^\alpha$, $\alpha = x, y, z$, are Pauli matrices acting on site $j \in \mathbb{Z}$ of a linear chain. The phases h_j are in-

dependently drawn from a uniform distribution in $[-\pi, \pi)$. The Hamiltonian version of this model, obtained by substituting $J, g, h_j \mapsto \tau J, \tau g, \tau h_j$ in Eq. (1) and taking the continuous-time limit $\tau \rightarrow 0$, is similar to the model where MBL was rigorously established in the regime $g \ll 1$ [7]. MBL behavior is known to persist in the same regime for finite driving period $\tau > 0$ [8, 9, 34, 36, 37]. Setting $J = g$ in Eq. (1), ED studies indicate that the MBL phase extends to $|g| < g_* \approx 0.4$ [35]. For weaker disorder strength $|J| = |g| > g_*$ the disordered KIC is ergodic. In particular, at the self dual points $|J| = |g| = \pi/4$ signatures of chaotic behavior in spectral correlations have been obtained [38]. We note that other kicked Floquet models of MBL have been investigated [8, 37, 39].

Disorder-averaged influence matrix — The influence matrix encodes the full set of temporal correlations of local operators [29, 30]. To illustrate this, we consider the dynamical structure factor $\langle O_p(t) O_p(0) \rangle = \text{Tr}(\hat{F}^{-t} O_p \hat{F}^t O_p \rho^0)$ of a local observable $O_p = \mathbb{1} \otimes \cdots \otimes \mathbb{1} \otimes O \otimes \mathbb{1} \otimes \cdots \otimes \mathbb{1}$ acting on spin p , using Keldysh path integral representation, graphically illustrated in Fig. 1(a,b),

$$\langle O_p(t) O_p(0) \rangle = \sum_{\{\sigma_j^\tau\}, \{\bar{\sigma}_j^\tau\}} [O_p]_{\{\bar{\sigma}^t\}, \{\sigma^t\}} [O_p \rho^0]_{\{\sigma^0\}, \{\bar{\sigma}^0\}} \prod_j \prod_{\tau=0}^{t-1} W_{\sigma_j^{\tau+1} \sigma_j^\tau} W_{\bar{\sigma}_j^{\tau+1} \bar{\sigma}_j^\tau}^* e^{iJ(\sigma_j^\tau \sigma_{j+1}^{\tau+1} - \bar{\sigma}_j^\tau \bar{\sigma}_{j+1}^{\tau+1}) + ih_j(\sigma_j^\tau - \bar{\sigma}_j^\tau)} \quad (2)$$

where $W_{\sigma'\sigma} = \langle \sigma' | e^{ig\hat{\sigma}^x} | \sigma \rangle$. We say that configurations σ_j^τ associated with the operator \hat{F}^t are on the *forward* time path and those $\bar{\sigma}_j^\tau$ associated with \hat{F}^{-t} on the *backward* path. The summation is over all spin trajectories $\{\sigma_j^\tau = \pm 1\}, \{\bar{\sigma}_j^\tau = \pm 1\}$ extending

$$\langle O_p(t) O_p(0) \rangle = \sum_{\{\sigma^\tau\}, \{\bar{\sigma}^\tau\}} \mathcal{I}_{L,p}[\{\sigma^\tau, \bar{\sigma}^\tau\}] \left([O]_{\bar{\sigma}^t \sigma^t} \prod_{\tau=0}^{t-1} W_{\sigma^{\tau+1} \sigma^\tau} W_{\bar{\sigma}^{\tau+1} \bar{\sigma}^\tau}^* e^{ih_p(\sigma^\tau - \bar{\sigma}^\tau)} [O \rho_p^0]_{\sigma^0 \bar{\sigma}^0} \right) \mathcal{I}_{R,p}[\{\sigma^\tau, \bar{\sigma}^\tau\}] \quad (3)$$

where we have denoted the result of the summation over spins on the left (right) as the left (right) *influence matrix* $\mathcal{I}_{L(R),p}$ acting on the forward and backward trajectories $\{\sigma^\tau\}, \{\bar{\sigma}^\tau\}$, $0 \leq \tau \leq t-1$ of spin p only. These objects, graphically represented in Fig. 1(a), capture the influence the rest of the system has on the dynamics of spin p . Clearly, expression (3) can be straightforwardly generalized to arbitrary time-ordered temporal correlations of local

from time $\tau = 0$ to $\tau = t$. Assuming that the initial density matrix $\rho^0 = \otimes_j \rho_j^0$ is a product operator, we formally perform the summation over trajectories of all spins on the left $\{\sigma_{j < p}^\tau\}, \{\bar{\sigma}_{j < p}^\tau\}$ and on the right $\{\sigma_{j > p}^\tau\}, \{\bar{\sigma}_{j > p}^\tau\}$ of spin p in Eq. (2), obtaining

operators $\langle O_p^{(n)}(t_n) \cdots O_p^{(1)}(t_1) \rangle$.

In a chain (or, more generally, in loop-free geometries), an influence matrix can be recursively computed from influence matrices of smaller subsystems, as illustrated from in Fig. 1(a,c). For a finite system of N spins, this can be concisely expressed by introducing transfer matrices \hat{T}_j acting along the space direction, i.e., $\mathcal{I}_{L,p} = \left(\prod_{j=1}^{p-1} \hat{T}_j \right) \mathcal{I}_0$ and $\mathcal{I}_{R,p} = \left(\prod_{j=N}^{p+1} \hat{T}_j \right) \mathcal{I}_0$, with

$$[T_j]_{\{\sigma, \bar{\sigma}\}, \{s, \bar{s}\}} = \left(\prod_{\tau=0}^{t-1} e^{iJ(\sigma^\tau s^\tau - \bar{\sigma}^\tau \bar{s}^\tau)} \right) e^{ih_j \sum_{\tau=0}^{t-1} (s^\tau - \bar{s}^\tau)} \left(\delta_{s^t \bar{s}^t} \prod_{\tau=0}^{t-1} W_{s^{\tau+1} s^\tau} W_{\bar{s}^{\tau+1} \bar{s}^\tau}^* [\rho_j^0]_{s^0 \bar{s}^0} \right), \quad (4)$$

and open boundary condition $\mathcal{I}_0[\{s, \bar{s}\}] \equiv 1$.

We are interested in disorder-averaged temporal correlations such as $\langle \langle O_p(t) O_p(0) \rangle \rangle$. Since the random field h_j is uncorrelated and equally distributed at each lattice site, the averaged transfer matrices $\langle \hat{T}_j \rangle = \hat{\mathcal{T}}$ are translationally invariant, provided the initial density matrices ρ_j^0 are the same. Unitarity of time evolution for a periodic chain of arbitrary size N gives $\text{Tr}(\hat{\mathcal{T}}^N) \equiv \langle \langle \mathbb{1} \rangle \rangle = 1$; hence, $\hat{\mathcal{T}}$ has a single non-vanishing and non-degenerate eigenvalue equal to 1. The “bulk” disorder-averaged influence matrix $\langle \mathcal{I} \rangle = \hat{\mathcal{T}}^\ell \mathcal{I}_0$, with $\ell > t$, is thus real [40], and can be identified with the single eigenvector of $\hat{\mathcal{T}}$, i.e., by the characteristic *self-consistency equation*

$$\hat{\mathcal{T}} \langle \mathcal{I} \rangle = \langle \mathcal{I} \rangle. \quad (5)$$

Due to the absence of correlations in the initial state and the strictly linear light-cone effect in this Floquet model, finite-size effects are present only at a distance $\ell \leq t$ from the boundaries [41].

Disorder averaging in model (1) can be carried out explicitly [38]: since disorder is random in space but uniform in time, averaging introduces non-local

in time “interactions”. Indeed, integrating over h_j in Eq. (4) transforms the corresponding phase term into a constraint $\delta(\sum_{\tau=0}^{t-1} (s^\tau - \bar{s}^\tau)) \equiv \delta_{M, \bar{M}}$, which couples the configurations of the considered spin between all times. Such a term cancels interference between forward and backward trajectories with different total magnetization $M \neq \bar{M}$, and is responsible for the development of long-range temporal correlations in the MBL phase.

MPS approach and temporal entanglement — To gain an insight into the structure of the IM in the MBL phase, we approximate the solution of the self-consistency equation (5) by an MPS ansatz with a maximal bond dimension χ . The reliability of this approximation depends on the amount of “bipartite entanglement” in the IM interpreted as a many-body “wavefunction” in the 4^t -dimensional space of forward/backward spin trajectories. This *temporal entanglement* (TE) may be considered as a quantifier of the system’s dynamics computational complexity.

Previously, we have shown [29] that the maximal (half-chain) von Neumann entanglement entropy $S(t/2)$ of the infinite-temperature folded IM —

obtained by considering $\sigma^\tau, \bar{\sigma}^\tau$ as a single 4-dit, cf. Fig. 1(a-c) — is exactly zero when $|J| = |g| = \pi/4$ for any h_j [42] thanks to the fact that the system acts as a perfectly dephasing (PD) Markovian bath. However, detuning away from these PD points, the entanglement $S(t/2)$ acquires “volume-law” scaling with t , albeit with a prefactor that vanishes as those points are approached. This scaling is expected to be a generic feature of thermalizing phases, and generally prevents MPS description from being efficient at long times, except near “special” points [29].

In contrast, we find that MPS methods remain efficient in the MBL phase up to long times, thanks to the slow scaling of TE. To implement MPS algorithms, we work in the folded picture [29, 32, 43]. The disorder-averaged transfer matrix $\hat{\mathcal{T}}$ is represented as a matrix product operator (MPO), which consists of the diagonal two-site matrices W , the global projection operator $\delta_{M,\bar{M}}$ originating from averaging over the random phase h , and the factorized operator dependent on the interaction strength J [see Eq. (4)]. The first and last operators can be expressed as MPOs with bond dimension 4 and 1, respectively. The projection operator can be expressed as a MPO with maximal bond dimension t [44]. Thus, the maximal bond dimension of $\hat{\mathcal{T}}$ is $4t$.

To find the IM one can iteratively apply the transfer matrix to the boundary vector \mathcal{S}_0 . This approach was used to obtain the ED results, but it does not yield a good approximation of the optimal MPS at a fixed bond dimension, mainly due to the relatively large bond dimension of the MPO. To mitigate this problem we refine the MPS afterwards by using the density matrix renormalization group (DMRG) algorithm [45]. We estimated the quality of the MPS representation using several metrics [44], including the proximity of the eigenvalue obtained from DMRG to the exact value 1 (see Fig. 1(e)).

We have used a combination of the MPS method and ED to analyze the infinite-temperature IM’s TE across the MBL transition in model (1), see Fig. 1(d). In the ergodic phase, TE increases fast with t , similarly to generic non-disordered thermal systems [29], which restricts us to the ED approach and thus limited time. However, this behavior drastically changes in the MBL phase, where TE exhibits an initial rise followed by a crossover to a very slow growth. Interestingly, the crossover occurs at longer times at smaller values of g . We remark that the TE patterns in the MBL phase and near PD points are qualitatively different: in [44], we show that TE of unfolded IM remains low in the former case, and is high in the latter case.

MBL and temporal long-range order — The IM contains information about the full *disorder-averaged* quantum noise spectrum of a system, allowing for a computation of time-dependent correlation functions. Here we consider the infinite temperature correlator of the local magnetization, $\langle\langle \hat{\sigma}_p^z(t) \hat{\sigma}_p^z(0) \rangle\rangle$, whose long-time behavior provides a direct probe of ergodicity breakdown in the MBL phase, widely used in experiments [14]; in this case, this correlator does not decay to zero as $t \rightarrow \infty$, indicating remanent magnetization. From a theory standpoint, the time-averaged remanent magnetization is of key importance, since it reflects the emergence of LIOMs, providing a dynamical order parameter of MBL [46]. Analysis of this quantity [47] is challenging due to inevitable presence of rare resonances, which have to be treated non-perturbatively [7]. In contrast, disorder-averaged IM contains the contribution of all resonances that are effective up to time t . Using formula (3) and the MPS representation of the IM obtained by DMRG, we calculate the disorder-averaged correlator $\langle\langle \hat{\sigma}^z(t) \hat{\sigma}^z(0) \rangle\rangle$ [Fig. 2(a)]. We observe that at strong disorder the magnetization saturates to a finite value, signalling MBL, while in the critical region it continues decaying at accessible time scales. Note that increasing bond dimension from $\chi = 128$ to $\chi = 256$ gives rise to a slower decay of magnetization. This indicates that $\chi = 128$ is not sufficient to faithfully capture the IM in the critical region, where, as seen in Fig. 1(d), TE is relatively high.

Next, we inquire into the difference of the IM between the MBL and the ergodic phase. The general structure of the IM of a thermalizing bath has been studied for an ensemble of non-interacting harmonic oscillators [30, 31], and more recently for quantum spin chains [29]. In this case the IM strongly suppresses “quantum” trajectories where $\sigma^\tau \neq \bar{\sigma}^\tau$, behaving similarly to a source of classical noise. This causes the system to damp local quantum-interference effects and dephase its spins, thus erasing local memory after a finite correlation time. An MBL system, in contrast, does not act as an efficient bath upon itself, producing quantum noise that does not fully erase local memory of initial states. We find that here the quantum trajectories are only weakly suppressed, reflecting the key role of persistent interference processes.

The onset of remanent magnetization can be linked to the appearance of temporal long-range order in the IM. To that end, we write $\langle\langle Z \rangle\rangle \equiv$

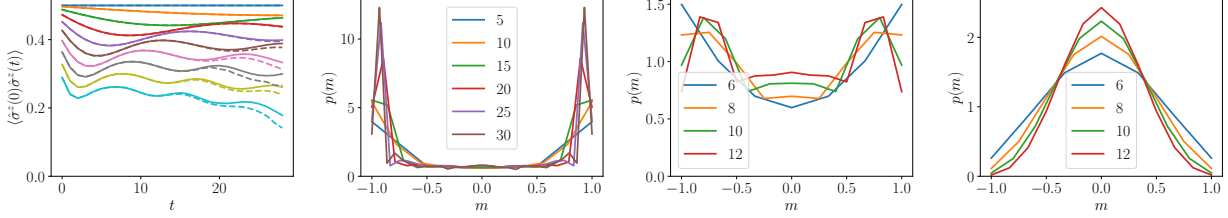


Figure 2. (a) Remanent magnetization $\langle\langle\hat{\sigma}^z(0)\hat{\sigma}^z(t)\rangle\rangle$ for different disorder strength equally spaced along the line $J = g = 0.04 \dots 0.35$ (top to bottom curves). These computations were performed at bond dimensions $\chi = 256$ (solid) and $\chi = 128$ (dashed). Note that the computations are well-converged at stronger disorder, while in the critical regime ($g = 0.35$) increasing bond dimension slows down the magnetization decay, indicating that there $\chi = 128$ is not sufficient to faithfully approximate IM. (b-d) Probability density $p(m)$ of time-averaged magnetization sectors in the ensemble of local spin trajectories defined by the IM: in the MBL phase ($J = g = 0.27$) (b), in the transition region ($J = g = 0.47$) (c), and in the ergodic phase ($J = g = 0.71$) (d). Different curves correspond to different evolution times, specified in the legend.

$\lim_{t \rightarrow \infty} \frac{1}{t} \sum_{\tau=1}^t \langle\langle\hat{\sigma}_j^z(\tau)\hat{\sigma}_j^z(0)\rangle\rangle$ as follows:

$$\langle\langle Z \rangle\rangle = \lim_{t \rightarrow \infty} \frac{1}{2t^2} \sum_{\tau, \tau'=0}^t \sum_{\{\sigma^s\}, \{\bar{\sigma}^s\}} \sigma^\tau \sigma^{\tau'}$$

$$\times \delta\left(\sum_s (\sigma^s - \bar{\sigma}^s)\right) \prod_s W_{\sigma^{s+1}, \sigma^s} W_{\bar{\sigma}^{s+1}, \bar{\sigma}^s}^* \langle\mathcal{I}\rangle^2[\{\sigma, \bar{\sigma}\}],$$

[cf. Eq. (3)] where we took into account that left and right IM are equal to $\langle\mathcal{I}\rangle$. Next, we represent the r-

h.s. of Eq. (6) as a sum over sets of trajectories with fixed magnetization $M = \sum_s \sigma^s = \sum_s \bar{\sigma}^s$ [48]. That enables us to take the sum over τ, τ' , which, within a given magnetization sector, yields M^2 . Thus,

$$(6)\langle\langle Z \rangle\rangle = \lim_{t \rightarrow \infty} \sum_{M=-t}^t (M/t)^2 P(M) = \int_{-1}^1 dm m^2 p(m), \quad (7)$$

where

$$P(M) = \lim_{t \rightarrow \infty} \frac{1}{2} \sum_{\{\sigma^s\}, \{\bar{\sigma}^s\}} \delta\left(\sum_s \bar{\sigma}^s - M\right) \delta\left(\sum_s \sigma^s - M\right) \prod_s W_{\sigma^{s+1}, \sigma^s} W_{\bar{\sigma}^{s+1}, \bar{\sigma}^s}^* \langle\mathcal{I}\rangle^2[\{\sigma, \bar{\sigma}\}], \quad (8)$$

is a positive “weight” representing the sum over trajectories in the sector with magnetization M . If the influence matrix is given as MPS, $P(M)$ can be expressed as a contraction with another MPS that implements the constraint $\delta(\sum_s \bar{\sigma}^s - M) \delta(\sum_s \sigma^s - M)$. Unitarity dictates that $\sum_M P(M) = 1$, and therefore $P(M)$ may be viewed as a probability. For convenience, we switch to the magnetization density $m = M/t$ in time and rescaled the probability density $p(m) = t P(M)$.

Expression (7) gives a necessary and sufficient criterion for MBL: ergodicity is broken, and local integrals of motion exist, if the probability distribution $p(m)$ for the time-averaged magnetization of individual-spin trajectories has a finite width in the infinite-time limit. In the ergodic phase, the width of $p(m)$ shrinks around its average $m = 0$ as $1/t$,

satisfying central limit theorem scaling. We confirmed this by an exact computation at the self-dual points, which gives a binomial distribution $P(M) = 2^{-t} \binom{t+M}{t}^{1/2}$. However, as the MBL phase is approached, $p(m)$ develops two symmetric peaks at finite values $\pm m^*$. This highlights that the MBL phase dynamically breaks the \mathbb{Z}_2 -symmetry of the disorder-averaged chain: Selecting “up” or “down” boundary conditions for the trajectory (i.e., initial and final state of spin p) produces a finite bias in the average magnetization towards the positive or negative side, respectively.

In Fig. 2(b-d) we report the results for the distribution $p(m)$ obtained with MPS for the MBL phase, and by ED at the transition and in the ergodic phase. It is apparent that $p(m)$ follows the above expectations, developing increasingly sharp peaks close to

$m = \pm 1$ in the MBL phase as the observation time window t is enlarged [panel (b)]; in contrast, in the ergodic phase [panel (d)], the distribution is single-peaked at $m = 0$ and narrows as t is increased. In the critical region between them [panel (c)], a peak at $m = 0$ is observed which slowly develops upon increasing t , reflecting the tendency to restoring thermal behavior at long times.

Summary and outlook — We have characterized a many-body, disordered system via its influence matrix, which fully describes its properties as a quantum bath. This approach allows for exact disorder averaging, therefore incorporating effects of rare regions on MBL. The slow increase of temporal entanglement in the MBL phase reflects that the system fails to act as a thermal bath on itself, and opens the door to efficient tensor-network approaches. We have implemented a proof-of-principle MPS algorithm and used it to extract time-dependent correlation functions that provide a benchmark for current quantum simulation experiments.

Looking forward, the slow entanglement scaling of IM in the MBL phase paves the way to constructing variational, and possibly exact, solutions for the self-consistency equation (5) in the limit $t \rightarrow \infty$. Such a solution, and its breakdown at weaker disorder due to proliferating resonances, will shed new light on MBL and the MBL-thermal transition. Finally, further applications of the IM approach may include other form of ergodicity breaking such as quantum scars, time crystals as well as circuits that combine unitary evolution with measurements or dissipation. Preliminary results [49] indicate that the temporal entanglement decreases when dissipation is added, broadening the applicability of our method.

Acknowledgments — We thank S. Choi, S. Garratt and L. Piroli for insightful discussions. A.L. acknowledges valuable discussions with G. Giudici and F. M. Surace on tensor-network implementations. The MPS computations in this work were performed using TeNPy [50]. This work is supported by the Swiss National Science Foundation and by the European Research Council (ERC) under the European Union’s Horizon 2020 research and innovation program (Grant Agreement No. 864597).

* These two authors contributed equally to this work

[1] R. Nandkishore and D. A. Huse, *Annual Review of Condensed Matter Physics* **6**, 15 (2015).
 [2] D. A. Abanin, E. Altman, I. Bloch, and M. Serbyn, *Rev. Mod. Phys.* **91**, 021001 (2019).
 [3] E. Altman, *Nature Physics* **14**, 979 (2018).

[4] M. Serbyn, Z. Papić, and D. A. Abanin, *Phys. Rev. Lett.* **111**, 127201 (2013).
 [5] D. A. Huse, R. Nandkishore, and V. Oganesyan, *Phys. Rev. B* **90**, 174202 (2014).
 [6] V. Ros, M. Müller, and A. Scardicchio, *Nuclear Physics B* **891**, 420 (2015).
 [7] J. Z. Imbrie, *Journal of Statistical Physics* **163**, 998 (2016).
 [8] P. Ponte, Z. Papić, F. Huveneers, and D. A. Abanin, *Phys. Rev. Lett.* **114**, 140401 (2015).
 [9] A. Lazarides, A. Das, and R. Moessner, *Phys. Rev. Lett.* **115**, 030402 (2015).
 [10] P. Bordia, H. Lüschen, U. Schneider, M. Knap, and I. Bloch, *Nature Physics* **13**, 460 (2017).
 [11] R. Moessner and S. L. Sondhi, *Nature Physics* **13**, 424 (2017).
 [12] B. Bauer and C. Nayak, *Journal of Statistical Mechanics: Theory and Experiment* **2013**, P09005 (2013).
 [13] J. Eisert, M. Cramer, and M. B. Plenio, *Rev. Mod. Phys.* **82**, 277 (2010).
 [14] M. Schreiber, S. S. Hodgman, P. Bordia, H. P. Lüschen, M. H. Fischer, R. Vosk, E. Altman, U. Schneider, and I. Bloch, *Science* **349**, 842 (2015).
 [15] J.-y. Choi, S. Hild, J. Zeiher, P. Schauß, A. Rubio-Abadal, T. Yefsah, V. Khemani, D. A. Huse, I. Bloch, and C. Gross, *Science* **352**, 1547 (2016).
 [16] A. Lukin, M. Rispoli, R. Schittko, M. E. Tai, A. M. Kaufman, S. Choi, V. Khemani, J. Léonard, and M. Greiner, *Science* **364**, 256 (2019).
 [17] J. Smith, A. Lee, P. Richerme, B. Neyenhuis, P. W. Hess, P. Hauke, M. Heyl, D. A. Huse, and C. Monroe, *Nat. Phys.* **12**, 907 (2016).
 [18] B. Chiaro, C. Neill, A. Bohrdt, M. Filippone, F. Arute, K. Arya, R. Babbush, D. Bacon, J. Bardin, R. Barends, S. Boixo, D. Buell, B. Burkett, Y. Chen, Z. Chen, R. Collins, A. Dunsworth, E. Farhi, A. Fowler, B. Foxen, C. Gidney, M. Giustina, M. Harrigan, T. Huang, S. Isakov, E. Jeffrey, Z. Jiang, D. Kafri, K. Kechedzhi, J. Kelly, P. Klimov, A. Korotkov, F. Kostritsa, D. Landhuis, E. Lucero, J. McClean, X. Mi, A. Megrant, M. Mohseni, J. Mutus, M. McEwen, O. Naaman, M. Neeley, M. Niu, A. Petukhov, C. Quintana, N. Rubin, D. Sank, K. Satzinger, A. Vainsencher, T. White, Z. Yao, P. Yeh, A. Zalcman, V. Smelyanskiy, H. Neven, S. Gopalakrishnan, D. Abanin, M. Knap, J. Martinis, and P. Roushan, “Direct measurement of non-local interactions in the many-body localized phase,” (2020), arXiv:1910.06024 [cond-mat.dis-nn].
 [19] W. De Roeck and F. m. c. Huveneers, *Phys. Rev. B* **95**, 155129 (2017).
 [20] A. Pal and D. A. Huse, *Phys. Rev. B* **82**, 174411 (2010).
 [21] D. J. Luitz, N. Laflorencie, and F. Alet, *Phys. Rev. B* **91**, 081103 (2015).
 [22] X. Yu, D. J. Luitz, and B. K. Clark, *Phys. Rev. B* **94**, 184202 (2016).
 [23] M. Serbyn, Z. Papić, and D. A. Abanin, *Phys. Rev. B* **96**, 104201 (2017).

- [24] A. Chandran, J. Carrasquilla, I. H. Kim, D. A. Abanin, and G. Vidal, Phys. Rev. B **92**, 024201 (2015).
- [25] M. Serbyn, A. A. Michailidis, D. A. Abanin, and Z. Papić, Phys. Rev. Lett. **117**, 160601 (2016).
- [26] F. Pollmann, V. Khemani, J. I. Cirac, and S. L. Sondhi, Phys. Rev. B **94**, 041116 (2016).
- [27] T. B. Wahl, A. Pal, and S. H. Simon, Phys. Rev. X **7**, 021018 (2017).
- [28] M. C. Bañuls, N. Y. Yao, S. Choi, M. D. Lukin, and J. I. Cirac, Phys. Rev. B **96**, 174201 (2017).
- [29] A. Leroose, M. Sonner, and D. A. Abanin, “Influence matrix approach to many-body floquet dynamics,” (2020), arXiv:2009.10105 [cond-mat.str-el].
- [30] R. Feynman and F. Vernon, Annals of Physics **24**, 118 (1963).
- [31] A. J. Leggett, S. Chakravarty, A. T. Dorsey, M. P. A. Fisher, A. Garg, and W. Zwerger, Rev. Mod. Phys. **59**, 1 (1987).
- [32] M. C. Bañuls, M. B. Hastings, F. Verstraete, and J. I. Cirac, Phys. Rev. Lett. **102**, 240603 (2009).
- [33] We note that for problems with discrete disorder potential, an alternative tensor-network approach to disorder averaging exists [51].
- [34] L. Zhang, V. Khemani, and D. A. Huse, Phys. Rev. B **94**, 224202 (2016).
- [35] M. Sonner, M. Serbyn, Z. Papić, and D. A. Abanin, “Thouless energy in a floquet model of many-body localization,” (2020), to appear.
- [36] D. A. Abanin, W. D. Roeck, and F. Huveneers, Annals of Physics **372**, 1 (2016).
- [37] C. Sündershauf, D. Pérez-García, D. A. Huse, N. Schuch, and J. I. Cirac, Phys. Rev. B **98**, 134204 (2018).
- [38] B. Bertini, P. Kos, and T. c. v. Prosen, Phys. Rev. Lett. **121**, 264101 (2018).
- [39] A. Chan, A. De Luca, and J. T. Chalker, Phys. Rev. Lett. **121**, 060601 (2018).
- [40] By virtue of the \mathbb{Z}_2 symmetry of the model.
- [41] Mathematically, this means that the null subspace of $\tilde{\mathcal{T}}$ fractures into nilpotent Jordan blocks of size $\leq t$.
- [42] L. Piroli, B. Bertini, J. I. Cirac, and T. c. v. Prosen, Phys. Rev. B **101**, 094304 (2020).
- [43] A. Müller-Hermes, J. I. Cirac, and M. C. Bañuls, New Journal of Physics **14**, 075003 (2012).
- [44] See Supplemental online material for details on the numerical methods used in the main text. Contains references [52, 53].
- [45] U. Schollwöck, Annals of physics **326**, 96 (2011).
- [46] A. Chandran, I. H. Kim, G. Vidal, and D. A. Abanin, Phys. Rev. B **91**, 085425 (2015).
- [47] V. Ros and M. Müller, Phys. Rev. Lett. **118**, 237202 (2017).
- [48] We remind that the delta-function there originates from disorder-averaging, which effectively cancels out interference terms between sectors with different magnetization.
- [49] M. Sonner, A. Leroose, and D. A. Abanin, in preparation.
- [50] J. Hauschild and F. Pollmann, SciPost Phys. Lect. Notes , 5 (2018), code available from <https://github.com/tenpy/tenpy>, arXiv:1805.00055.
- [51] B. Paredes, F. Verstraete, and J. I. Cirac, Phys. Rev. Lett. **95**, 140501 (2005).
- [52] T. L. Lezama, S. Bera, and J. H. Bardarson, Physical Review B **99**, 161106 (2019).
- [53] E. Stoudenmire and S. R. White, New Journal of Physics **12**, 055026 (2010).

Supplemental Material

Characterizing many-body localization via exact disorder-averaged quantum noise

Michael Sonner,^{1,*} Alessio Lerose,^{1,*} and Dmitry A. Abanin¹

¹*Department of Theoretical Physics, University of Geneva,
Quai Ernest-Ansermet 24, 1205 Geneva, Switzerland*

(Dated: January 3, 2022)

In this Supplemental Material, we provide additional details on the numerical calculations used in the main text.

EXACT DIAGONALIZATION

As a benchmark for MPS calculations and to explore the ergodic side of the MBL transition, we employ an exact diagonalization (ED) code. To this end, we interpret the influence matrix (IM) $\mathcal{S}[\{\sigma, \bar{\sigma}\}]$ as a “wavefunction” in the 2^{2t} -dimensional vector space spanned by the basis $\{|\sigma_0 = \pm, \dots, \sigma_{t-1} = \pm, \bar{\sigma}_{t-1} = \pm, \dots, \bar{\sigma}_0 = \pm\rangle\}$. Accordingly, we express the transfer matrix $[\mathcal{T}]_{\{\sigma, \bar{\sigma}\}, \{s, \bar{s}\}}$ in Eq. (5) of the main text [obtained by taking the average of Eq. (4) of the main text over the random phase h_j] as a product of three operators,

$$\hat{\mathcal{T}} = \hat{\mathcal{V}} \hat{\mathcal{P}} \hat{\mathcal{W}}, \quad (\text{S1a})$$

$$[\mathcal{V}]_{\{\sigma, \bar{\sigma}\}, \{s, \bar{s}\}} = \prod_{\tau=0}^{t-1} \exp(iJ\sigma^\tau s^\tau) \prod_{\tau=0}^{t-1} \exp(-iJ\bar{\sigma}^\tau \bar{s}^\tau), \quad (\text{S1b})$$

$$[\mathcal{P}]_{\{\sigma, \bar{\sigma}\}, \{s, \bar{s}\}} = \prod_{\tau=0}^{t-1} \delta_{\sigma^\tau s^\tau} \prod_{\tau=0}^{t-1} \delta_{\bar{\sigma}^\tau \bar{s}^\tau} \left(\delta_{\sum_{\tau=0}^{t-2} s^\tau, \sum_{\tau=0}^{t-2} \bar{s}^\tau} \right), \quad (\text{S1c})$$

$$[\mathcal{W}]_{\{\sigma, \bar{\sigma}\}, \{s, \bar{s}\}} = \prod_{\tau=0}^{t-1} \delta_{\sigma^\tau s^\tau} \prod_{\tau=0}^{t-1} \delta_{\bar{\sigma}^\tau \bar{s}^\tau} \left(\delta_{s_{t-1} \bar{s}_{t-1}} \prod_{\tau=0}^{t-2} W_{s^{\tau+1} s^\tau} W_{\bar{s}^{\tau+1} \bar{s}^\tau}^* \rho_{s^0 \bar{s}^0}^0 \right), \quad (\text{S1d})$$

where $W_{\sigma' \sigma} = \langle \sigma' | e^{ig\hat{\sigma}^x} | \sigma \rangle \equiv \cos g \delta_{\sigma', \sigma} + i \sin g \delta_{\sigma', -\sigma}$. This representation is illustrated in Fig. S1-(a,b). We note that the last kick has been erased compared to Fig. 1-(c) of the main text, exploiting its unitarity; a further simplification can be done to the first longitudinal field when $\rho^0 = \mathbb{1}/2$ (infinite-temperature ensemble), imposing $s^0 = \bar{s}^0$ in $\hat{\mathcal{P}}$. The combination of these two operations decreases the total dimensionality of the input and output vector space by a factor 4.

The matrices $\hat{\mathcal{W}}$ and $\hat{\mathcal{P}}$ are diagonal in the computational basis, which we can interpret as the $\hat{\sigma}^z$ product basis for our chain of $2t$ spins-1/2. Within this interpretation, the operator $\hat{\mathcal{V}}$ is diagonal in the $\hat{\sigma}^x$ product basis. We exploit this fact for an efficient implementation of the applications of $\hat{\mathcal{T}}$ via the Fast Walsh Hadamard transformation (FWHT)^{S1}, which can be used to convert between these two bases with $\mathcal{O}(t2^{2t-1})$ basic operations. Note that the FWHT is an involution. The algorithm to apply $\hat{\mathcal{T}}$ to an arbitrary vector thus reads:

1. multiply its components by the diagonal components of $\hat{\mathcal{P}}$ and $\hat{\mathcal{W}}$;
2. apply FWHT;
3. multiply the vector’s components by the (now diagonal) components of $\hat{\mathcal{V}}$;
4. apply FWHT again.

To find the thermodynamic-limit IM we simply use this procedure t times starting from the boundary vector $\mathcal{S}_0[\{s, \bar{s}\}] \equiv 1$. For the infinite-temperature initial ensemble, $t/2$ iterations suffice. This algorithm spares us from constructing and diagonalizing $\hat{\mathcal{T}}$, thus allowing us to push our ED results up to $t = 12$ with modest resources.

MATRIX PRODUCT STATES

For the matrix product state (MPS) method, we choose to work in the folded picture where each spin on the forward trajectory is paired up with its corresponding spin on the backward trajectory such that they form a 4-dimensional local space^{S2}. This gives an open chain geometry, thus avoiding complications arising from periodic

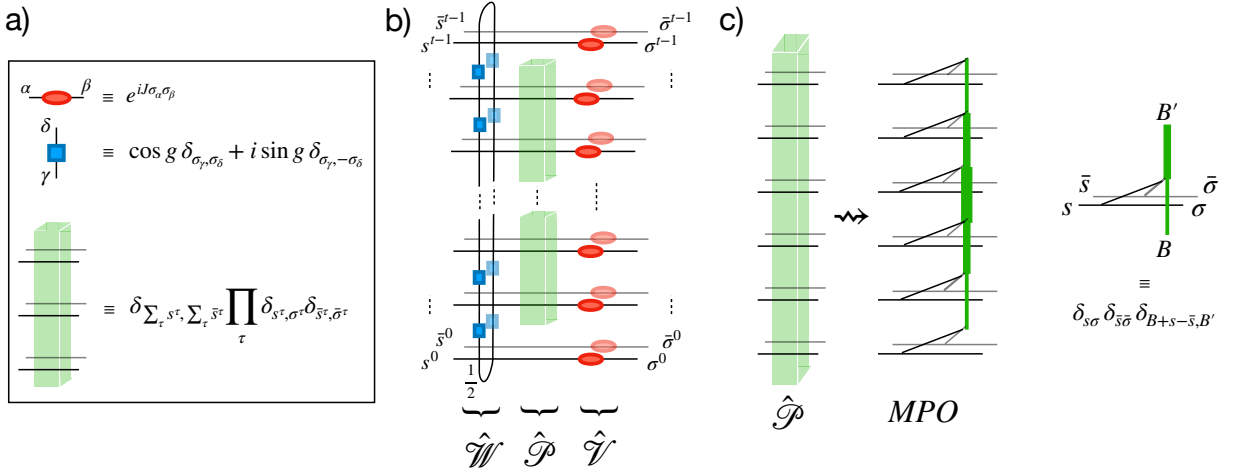


FIG. S1. Panels a), b): Graphical representation of Eqs. (S1). Panel c): Graphical illustration of the MPO representation of \hat{P} in Eq. (S4)

boundary conditions of the closed Keldysh contour, present in the unfolded representation. We label and order the basis vectors of this local space by $S = (s, \bar{s}) = (\uparrow, \uparrow), (\downarrow, \downarrow), (\uparrow, \downarrow), (\downarrow, \uparrow)$. It is straightforward to write the factors \hat{V} and \hat{W} in the transfer matrix decomposition in Eq. (S1) as matrix product operators (MPOs) of bond dimensions 1 and 4, respectively:

$$\begin{aligned}
 [\mathcal{V}]_{\{S^\tau\}, \{\Sigma^\tau\}} &= \prod_{\tau=0}^{t-1} \begin{pmatrix} 1 & 1 & e^{-2iJ} & e^{2iJ} \\ 1 & 1 & e^{2iJ} & e^{-2iJ} \\ e^{-2iJ} & e^{2iJ} & 1 & 1 \\ e^{2iJ} & e^{-2iJ} & 1 & 1 \end{pmatrix}_{S^\tau, \Sigma^\tau} \quad (S2) \\
 [\mathcal{W}]_{\{S^\tau\}, \{\Sigma^\tau\}} &= \sum_{\{A^\tau\}} \mathbb{1}_{A^t} \prod_{\tau=0}^{t-1} \begin{pmatrix} \cos^2 g & \sin^2 g & i \sin g \cos g & -i \sin g \cos g \\ \sin^2 g & \cos^2 g & -i \sin g \cos g & i \sin g \cos g \\ i \sin g \cos g & -i \sin g \cos g & \cos^2 g & \sin^2 g \\ -i \sin g \cos g & i \sin g \cos g & \sin^2 g & \cos^2 g \end{pmatrix}_{A^{\tau+1}, A^\tau} \delta_{A^\tau, S^\tau} \delta_{S^\tau, \Sigma^\tau} \rho_{A^0}^0 \quad (S3)
 \end{aligned}$$

In the second equation, the labels $\{A^\tau = (a^\tau, \bar{a}^\tau)\}$ of virtual bonds run over the bases of four-dimensional ancillary spaces isomorphic to the local folded spin spaces. The projection operator \hat{P} which arises from disorder averaging can be represented as a MPO with maximum bond dimension t . Here the virtual index B^T on each bond $(T, T+1)$ represents the difference in magnetization $\sum_{\tau=0}^T s^\tau - \bar{s}^\tau$ between the portions of forward and backward paths to the left of this bond. In other words, the local matrices

$$P_{B^\tau, B^{\tau+1}}^{S^\tau, \Sigma^\tau} = \delta_{S^\tau, \Sigma^\tau} \delta_{B^\tau + s^\tau - \bar{s}^\tau, B^{\tau+1}} \quad (S4)$$

composing the MPO, read the incoming virtual index B^τ and add the local magnetization difference $s^\tau - \bar{s}^\tau$ to it to produce the outgoing virtual index $B^{\tau+1}$. The value of the virtual index B^τ can thus remain unchanged, increase by one or decrease by one when proceeding to $B^{\tau+1}$, making the local bond dimension $\chi_\tau = 2\tau + 1$. Since \hat{P} globally projects onto the zero magnetization sector $\sum_\tau (s^\tau - \bar{s}^\tau) = 0$, we only need to carry virtual indices which are consistent with this sector. Thus the maximal bond dimension is t at the central bond(s) of the chain. This MPO is represented in Fig. S1(c).

Due to the large bond dimension it is not possible to iteratively apply the transfer matrix MPO for \hat{T} to an MPS at once and compress the result. Instead the MPS needs to be compressed during the application of the MPO, using the zip-up method^{S3}. We can improve the iterative MPS by feeding it into a two-site DMRG code where we target the eigenvector with largest absolute eigenvalue. As this method is variational, it avoids compounding errors in contrast to the iterative method^{S4}.

Different metrics of the quality of the MPS are displayed in Fig. S2. The role of energy in conventional DMRG is taken by the eigenvalue of the transfer matrix MPO in the last DMRG step. Due to the pseudo-projection property of \hat{T} (see the main text), the exact eigenvalue is 1. We can also inspect the discrepancy of the IM entry on classical

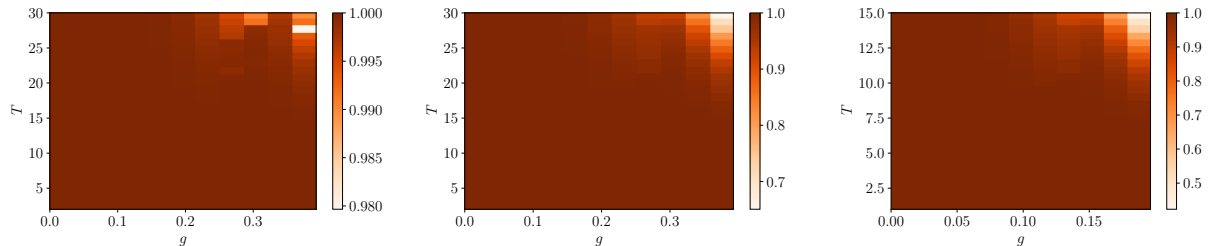


FIG. S2. Different metrics to assess the quality of the MPS representation of the IM, as a function of the model parameter $g = J$ and of the evolution time T . Left panel: DMRG eigenvalue of the transfer matrix; the exact value is 1 (see the main text). Middle panel: average IM elements of classical trajectories $\{\sigma = \bar{\sigma}\}$; the exact value of each of them is 1 (see Ref. S2). Right panel: expectation value of the identity matrix $\langle\langle \mathbb{1}(t)\mathbb{1}(0) \rangle\rangle$ [cf. Fig. 1-(a) of the main text] computed using the DMRG IM. For all the three metrics, depletion from the exact result is consistently observed for large T and large $J = g$.

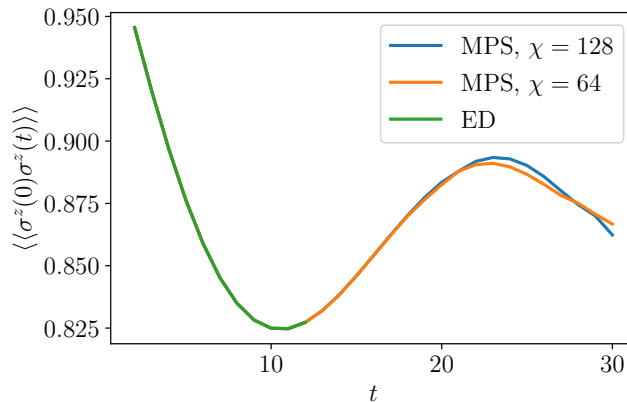


FIG. S3. Comparison between the evolution of the dynamical structure factor $\langle\langle \hat{\sigma}^z(t)\hat{\sigma}^z(0) \rangle\rangle$ computed with ED and MPS methods, for $J = g = 0.12$.

trajectories $\{\sigma = \bar{\sigma}\}$ from the exact value 1 (see Ref. S2). Last, we can compute the full path-integral of Fig. 1-(a) of the main text, with all observables of spin p set to identity, using the DMRG IMs. The exact value of this quantity is 1. We observe consistent deviations of the three metrics from their exact values for intermediate coupling strength (i.e., towards the MBL transition) and large times beyond the reach of ED, the last metric being the most sensitive. Furthermore, Fig. S3 shows the agreement between converged MPS data and ED data for the dynamical structure factor $\langle\langle \hat{\sigma}^z(t)\hat{\sigma}^z(0) \rangle\rangle$.

Lastly, we elucidate the differences in entanglement patterns between the MBL phase and the vicinity of PD points. Since both regions show low temporal entanglement (albeit scaling differently with the evolution time), it is legitimate to question the nature of this apparent similarity. The latter, however, disappears upon unfolding the IM wavefunction, as illustrated in Fig. S4. Here, we have the possibility to consider a bipartition separating forward and backward spins. The entanglement entropy $S_{f/b}(t)$ associated with such a bipartition is only low in the MBL phase, whereas it is large in the ergodic phase. At the self-dual point, in particular, we have $S_{f/b}(t) = (t + 1) \log 2$, because the IM wavefunction is a product state of $t + 1$ maximally entangled Bell pairs between each spin on the forward branch and its equal-time partner on the backward branch. This occurrence is interpreted as follows. In the MBL phase, there exist as much correlations between spins on the same time branch as between spins on opposite time branches. Conversely, ergodicity produces strong correlations between forward and backward trajectories: a manifestation of the suppression of quantum interference.

* These two authors contributed equally to this work

[S1] T. L. Lezama, S. Bera, and J. H. Bardarson, Physical Review B **99**, 161106 (2019).

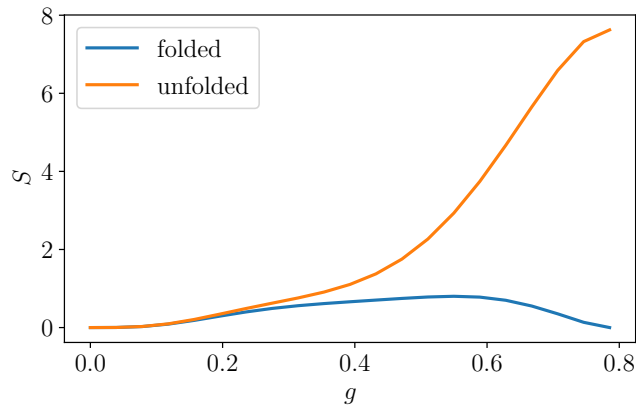


FIG. S4. Entanglement pattern across the MBL transition. Data are obtained from ED computations of the IMs for $t = 12$. The two curves show the bipartite entanglement entropy of the IM wavefunction corresponding to two structurally different bipartitions. The “folded” curve shows $S(t/2)$ of the folded IM, as in the main text; this quantity is low both near the fully decoupled line $J = 0$ and near the self-dual point $J = g = \pi/4$. The “unfolded” curve $S_{f/b}(t)$ corresponds instead to bipartitioning the chain into forward and backward spins; this quantity is only low in the MBL phase, but is very large in the ergodic phase.

- [S2] A. Lerosee, M. Sonner, and D. A. Abanin, “Influence matrix approach to many-body floquet dynamics,” (2020), [arXiv:2009.10105 \[cond-mat.str-el\]](https://arxiv.org/abs/2009.10105).
- [S3] E. Stoudenmire and S. R. White, *New Journal of Physics* **12**, 055026 (2010).
- [S4] U. Schollwöck, *Annals of physics* **326**, 96 (2011).